New Schiff base Derivatives Bearing Sulfonamide Moiety: Synthesis, *In vitro* Antimicrobial Activity, DFT Calculations, ADMET and Molecular Docking Study

Zerrouki, Samira [•]
Laboratoire de Physico-Chimie Théorique et de Chimie Informatique, Faculty of Chemistry, Houari Boumediene Sciences and Technology University, Algiers, ALGERIA

Bouchoucha, Afaf
Hydrometallurgy and Molecular Inorganic Chemistry Laboratory, Faculty of Chemistry, Houari Boumediene Sciences and Technology University, Algiers, ALGERIA

Djellouli, Fayrouz
Laboratoire de thermodynamique et de modélisation moléculaire, Faculty of Chemistry, Houari Boumediene Sciences and Technology University, Algiers, ALGERIA

Bouzaheur, Amal
Laboratoire de Physico-Chimie Théorique et de Chimie Informatique, Faculty of Chemistry, Houari Boumediene Sciences and Technology University, Algiers, ALGERIA

Si Larbi, Karima; Bourouai , Mohamed Amine
Hydrometallurgy and Molecular Inorganic Chemistry Laboratory, Faculty of Chemistry, Houari Boumediene Sciences and Technology University, Algiers, ALGERIA

Zaatar, Sihem [*+]
Laboratoire de Physico-Chimie Théorique et de Chimie Informatique, Faculty of Chemistry, Houari Boumediene Sciences and Technology University, Algiers, ALGERIA

ABSTRACT: *In the present work (E)-4-((4-(benzyloxy) benzylidene) amino)-N-(5-methylisoxazol-3-yl) benzenesulfonamide (L^1) and (E)-N-(5-methylisoxazol-3-yl)-4-((4-nitrobenzylidene) amino) benzenesulfonamide (L^2) have been successfully prepared in alcoholic medium with Hydrochloric* acid HCl as a catalytic agent. *L^1 and L^2 have been characterized by elemental analysis, FT-IR, 1H NMR, 13C-NMR, SM, and UV-visible spectroscopy. Theoretical calculations were performed at the DFT level of theory using the B3LYP functional and the 6-31G (d, p) basis set, and electronic properties were calculated using the Time-Dependent Density Functional Theory (TD-DFT) method. In addition to the optimized geometrical structure, Frontiers molecular orbital HOMO/LUMO and NBO charges have been investigated to describe the chemical reactivity*

* *To whom correspondence should be addressed.*
+ *E-mail: sihem.zaater@usthb.edu.dz*
1021-9986/2024/1/204-224 21/$/7.01
● *Another Address: Ecole Supérieur des Sciences Appliquées Alger (ESSA), place des martyrs, Algiers, Algeria.*

of the compounds. The vibrational wavenumbers were calculated and they correlated well with the experimental data. The antibacterial activity of the ligands was tested. The results revealed that the synthesized compound exhibited good to moderate antibacterial activity. Furthermore, interactions between synthesized compounds and bacterial proteins were evaluated by molecular docking while pharmacokinetics and toxicity were studied by ADMET analysis.

KEYWORDS: *Schiff base, Dulfamide derivative, DFT, In vitro antimicrobial activity, Molecular docking, ADMET analysis.*

INTRODUCTION

Figure ht against bacteria is necessary to protect humanity's health. Bacteria are constantly evolving genetically, which allows them to develop antibiotic resistance. For these reasons, the search for new antimicrobial chemical compounds is considered one of the most important areas in medicinal chemistry [1]. In recent years, researchers have given great importance to the synthesis and characterization of new drugs that exhibit broad biological activities such as antibacterial, antifungal, antimalarial, antituberculosis, antipyretic, anti-inflammatory, and antiviral properties [2-5]. Unfortunately, the global pandemic caused by SARS-CoV-2 (Severe Acute Respiratory Syndrome Coronavirus) has contributed to the rise of antibacterial resistance [6-8]. Sulfonamides are the oldest well-known category of antimicrobial agents commonly used against bacterial and fungal infections and contain pharmacological qualities as well as antibacterial activity; they received specific attention due to their medicinal use [9]. Sulfonamides are antibiotics that stop the growth of bacteria by interfering with PABA (para amino benzoic acid) and inhibiting the activity of the DHPS enzyme (dihydropteroate synthase). Against SARS-CoV-2, cyclic sulfonamides exhibit a remarkable reticence, according to recent scientific research [10, 11]. Another important class of organic compounds in medicine, are Schiff bases which are known as imines or azomethines which were discovered by Hugo Schiff in 1864. Schiff bases are used as substrates in the preparation of several industrial and biologically active compounds via ring closure, cycloaddition, and replacement reactions [12-14]. They have displayed a wide variety of biological actions such as antifungal, antibacterial, antimalarial, anti-inflammatory, antiproliferative, antiviral, and antipyretic qualities [11,12]. Schiff bases have also received a lot of attention due to their exceptional electrical and stunning tenability. Schiff bases are used in a variety of applications, including catalysts, polymer stabilizers, organic synthesis intermediates, pigments, and dyes [15,16]. Additionally, they are one of the most useful and extensively researched classes of ligands in coordination chemistry. Their derivatives are well known for a broad spectrum of natural pharmacological properties; the imine group present in these compounds is essential for their biological activities [17-20].

The aim of this work is the synthesis of new antimicrobial agents based on sulfonamide derivatives such as Schiff bases which exhibit excellent antibacterial activity against gram-positive germs. In this context and to develop new drugs, we report the synthesis and characterization of two new Schiff base sulfamide derivative compounds (E)-4-((4-(benzyloxy) benzylidene) amino)-N-(5-methylisoxazol-3-yl) benzenesulfonamide (L^1) and (E)-N-(5-methylisoxazol-3-yl)-4-((4-nitro benzylidene) amino) benzenesulfonamide (L^2) to have new compounds exhibiting biological activity. Theoretical calculations were completed at the DFT [20,21]**.** Finally, the synthesized compounds were tested for antibacterial and antifungal activities and a molecular Docking approach was performed to generate the binding pose and affinity between ligands and targets [20,21].

EXPERIMENTAL SECTION

Materials

All used reagents were of analytical grade; solvents (Merck) such as ethanol and Dimethyl Sulfoxide (DMSO) were used without purification. UV-Visible spectra were recorded in solution in DMSO using the JASCO V-630 UV-Vis spectrophotometer; IR spectra were recorded using a model Perkin Elmer Spectrum 65 FT-IR spectrometer

Table 1: Physical data for L^1, L^2

Compound	Exp (Calc.) %					Melting point (°C)	Color	Yield (%)
	C	H	N	S	O			
L^1	64.12 (64.42)	4.68 (4.73)	9.45 (9.39)	7.22 (7.16)	14.33 (14.30)	225	Light Yellow	85
L^2	52.55 (52.85)	3.73 (3.65)	14.37 (14.50)	8.41 (8.30)	20.65 (20.70)	227	Light Yellow	73

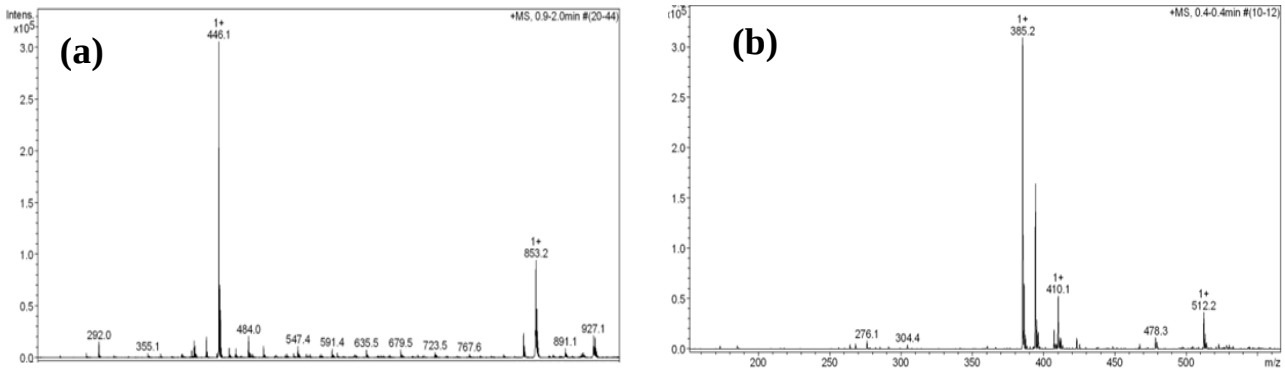

Fig. 1: Mass spectroscopy (a) for L^1 and (b) for L^2

using KBr discs in the spectral range 400 to 4000 cm^{-1}. The Nuclear magnetic resonance spectra 1H NMR were recorded in CDCl3 on Bruker NMR 400 MHz spectrometer and the chemical shifts are reported as δ values in parts per million (ppm) relative to tetramethylsilane (TMS) as reference solvent.

Synthetic method for synthesis of Schiff bases (L^1, L^2)

The ligands L^1 and L^2 were synthesized following the well-known reaction of Schiff base formation which consists of a condensation reaction of a primary amine with an aldehyde or ketone. 10 mmol (2.533 g) of sulfamethoxazole alcohol solution (30 ml of absolute ethanol) was added to a warm alcohol solution of each of the two aldehydes: 10 mmol (1.733 g) of 4-(benzyloxy) benzaldehyde (L^1) and 4-nitrobenzaldehyde (L^2) (20 ml of absolute ethanol). A catalytic amount (5 drops) of Hydrochloric acid HCl was used. At 78°C, the two solutions are mixed in a 100 ml round-bottomed flask for 4 hours with vigorous stirring and then kept cold for 24 hours. The formed ligands were filtered in a vacuum and washed with a cold (50:50 v/v) mixture of distilled water. The reaction conditions are shown in (Scheme 1). The chemical structure of the synthesized compounds was performed by elemental analysis, FT-IR, ^{1}H NMR, ^{13}C-NMR, Mass spectroscopy (ESI method) Fig. 1, and UV-visible. Analysis calculated: C, 52.85; H, 3.65; N, 14.50; O,20.70; S, 8.30 (Table 1) [22,23].

L^1: Light yellow color solid, m p= 225 °C, yield= 85%, time= 75 minutes. FT-IR (cm^{-1}): 3290 (NH str.), 3000-2500 (CH), 1601 (C=N str. Oxazole ring), 1307 (SO2 asym.str.), 1159 (SO2 sym. str.),890 (SN Ar. sulfamide.), 1255, 1088, 1008 (C-N, C-O, N-O str. oxazole moiety), 1377,1466 (CH, CH2 and CH3 rocking deformations). ^{1}H NMR (400 MHz, DMSO) δ 2.31 (d, *J* = 0.7 Hz, 3H, CH3), 5.21 (s, 2H, CH2), 6.17 (d, *J* = 0.9 Hz, 1H, H-4'), 7.17 (d, *J* = 8.8 Hz, 2H, H-3'',5''), 7.44 – 7.34 (m, 5H, H-3, 5, 2''', 4''', 6'''), 7.48 (d, *J* = 7.0 Hz, 2H, H-3''', 5'''), 7.92 – 7.85 (m, 4H, H-2, 6, 2'', 6''), 8.53 (s, 1H, H-C=N), 11.39 (s, 1H,NH). 13C NMR (101 MHz, DMSO) δ 12.52 (CH3), 69.98 (CH2), 95.90 (C-4'), 115.69 (C-3'', 5''), 122.07 (C-2''', 6'''), 128.26 (C-3''', 5'''), 128.46 (C-4'''), 128.61 (C-2, 6), 128.95 (C-3, 5), 131.44 (C-2'', 6''), 132.26 (C-1''), 136.26 (C-1'''), 137.04 (C-1) , 156.55 (C-3'), 158.04 (C-4), 162.01 (C=N), 162.89 (C-4''), 170.80 (C-5').

L^2: Light Yellow color solid, m p= 227 °C, yield= 73%, time= 75 minutes. FT-IR (cm^{-1}): 3000,2500 (CH,CH2 str.), 3145(N-H .sulfamide), 1593 (C=N str. Oxazole ring), 1610 (C=N str. imine), 1590,1500(C=C .benzene ring), 1400,1500 (CH_2 and CH_3 rocking deformations) 1330 (SO_2 asym. str.) , 1138 (SO2 sym. str.), 1279 (C-N sym. str.),1095(C-O asym. str.),1026 (N-O asym. str.) , 929 (SN Ar. sulfonamide.). 1HNMR (DMSO-d6): δ 2.29-2.34 (s, 3H (C6)), 6.08 (s, 1H (C2), J= 8.4 Hz), 10.94 (s, 1H (N7), J=8 Hz), 9.94 (s, 1H (C18)), 5.24 (s, 2H (C26), J= 7.6 Hz), 6.78-8.02 (t, 8H (Cycle(1+2)).

In vitro antimicrobial activity

The *in vitro* antimicrobial and antifungal activity for L^1 and L^2 are tested by the agar-well diffusion method. This method was performed in Petri dishes with Sabouraud medium for fungi and Mueller Hinton agar for bacteria strains. The medium was seeded aseptically with a 10^6 CFU/mL suspension of young cultures of the tested bacteria and fungi. Standard drugs for antibacterial and antifungal activities were Gentamicin and ketoconazole respectively. The synthesized Schiff bases were prepared at 50 µg/mL in DMSO is applied to sterile discs (approximately 20 µL). The plates are then incubated at 37°C for 24 hours for bacterial strains and at 30°C for 48 hours for fungal strains. The diameter of the halo formed around the wells, known as the inhibition zone, is used to assess the inhibition effect of the tested strains. Generally, an active compound has an inhibition diameter greater than 8 mm [24].

DFT study

Theoretical calculations have been performed with the GAUSSIAN 09[25] program packaged to the gradient-corrected hybrid density functional B3LYP [22-30] using a 6-31G (d, p) basis set. The population analysis is obtained by the Natural Bond Orbital (NBO) program [31]. The ^{1}H NMR isotropic shielding is calculated using the GIAO (the Gauge–Including Atomic Orbital) method [32] at the same level of theory for both sulfonamides derivates concerning TMS (tetramethylsilane) as a reference solvent. Know that DFT is the most popular method due to its accuracy and also their computational cost. The characterization of excited states and electronic transitions was done by the Time-Dependent DFT (TD-DFT) method [33]. To reproduce the experimental electronic spectra ten first singlet excited states are generated.

Molecular docking

The products were subjected to a molecular docking simulation to determine the binding affinities and modes of the compounds with the bacterial receptors. A gram-negative bacterium, *Escherichia coli*, previously tested in vitro antimicrobial activity, was chosen for the molecular docking study to find a correlation between in vitro antimicrobial activity and silico protein-ligand interaction. The RCSB protein data bank was used to download the crystal structures of the target enzyme dihydropteroate synthase of *Escherichia coli* (PDB ID:1AJ0). The 1AJ0 protein was prepared with AutoDockTools (ADT), and molecular docking was completed with the AutoDock 4.2 program [34].

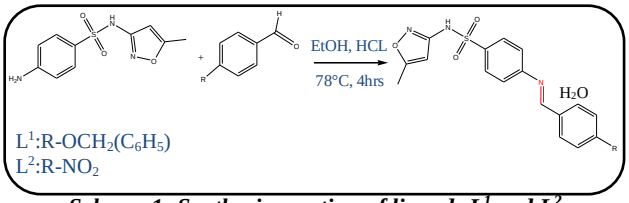

Scheme 1: Synthesis reaction of ligands L^1 and L^2

ADMET profiles and drug-likeness

The prediction of ADMET properties and drug-likeness was performed using SwissADME [35] and admetSAR servers [36]. Hence, the permeation through the blood-brain barrier (BBB), the Human Intestinal Absorption (HIA) capacity, $CaCo_2$ infiltration, and toxicity were determined. The Drug-likeness evaluation of the studied compounds was performed by testing their compliance with the well-known Lipinski rule [37] and then with Veber's rule [38].

RESULTS AND DISCUSSION

Chemistry

The Schiff base derivatives L^1, and L^2 were synthesized via a condensation reaction of amine with the two corresponding aldehydes by using DMSO as a solvent and Hydrochloric acid as a catalyst (Scheme 1).

Infrared spectroscopy

The experimental spectra of L^1 and L^2 exhibit the different bands of the functional groups present in the studied molecules. The characteristic bands were attributed and compared to the computed theoretical data. In the FT-IR spectrum for L^1, the characteristic absorption around 1601 cm^{-1} can be related to the stretching vibration of (-C=N) Schiff bases which could be a reasonable confirmation of Schiff base synthesis. The (N-H)sulfamide group stretching vibration band is observed at 3290 cm^{-1}. The asymmetric and symmetric vibration bands of the $-SO_2$ group appear in the region 1307 cm^{-1} and 1159 - 1108 cm^{-1} respectively. In the DFT calculated spectra, these bands are found at 1317cm^{-1} and 1142cm^{-1} for the asymmetric and symmetric vibrations respectively [39,40]. The band near 890 cm^{-1} is assigned to the (S-N) sulfamide bond. The deformation vibrations in the plane of the CH, CH2, and CH3 groups are observed at 1377-1466 cm^{-1} range [41,42].

Table 2: Selected IR frequencies ν(cm^{-1}) and assignments.

L^1			L^2		
Experimental	Theoretical		Experimental	Theoretical	
ν(cm^{-1})	ν(cm^{-1})	Assignement	ν(cm^{-1})	ν(cm^{-1})	Assignement
3290	3565	ν_sN-H	3145	3542	ν_sN-H
3000-2500	3004-3021	ν_sC-H in C-H and CH2	3000-2500	3059-3315	ν_sC-H in C-H and CH2
1579	1541	ν_s RingII C=N	1593	1538	ν_sRingI C=N
1601	1615	ν_sC=N$_{imine}$	1610	1630	ν_sC=N$_{imine}$
1307	1317	ν_{as}SO2	1590-1500	1609-1652	ν_sRingIII C=C
1159-1108	1142	ν_sSO2	1400-1500	1420-1497	CH2+ νδCH3
1255	1280	νC-N	1138-1330	1131-1305	ν_sS=O+$\nu_{\alpha s}$S=O
1088	1050	ν C-O	1279	1274	ν_sC-N
1008	1029	νN-O	1095	1044	ν_{as}C-O
1377-1466	1416-1425	δρRingIIICH+δρCH2+scδCH3	1026	1028	ν_{as}N-O
890	861	ν_sS-N	927	864	ν_sS-N

Abbreviations ν: bond stretching, δ: in-plane deformation, ρ: rocking, as: antisymmetric, s: symmetric, sc: scissoring, RingI: oxazole ring RingII: azomethine ring , RingIII: benzene ring and RingIIII: imine groupe ring .

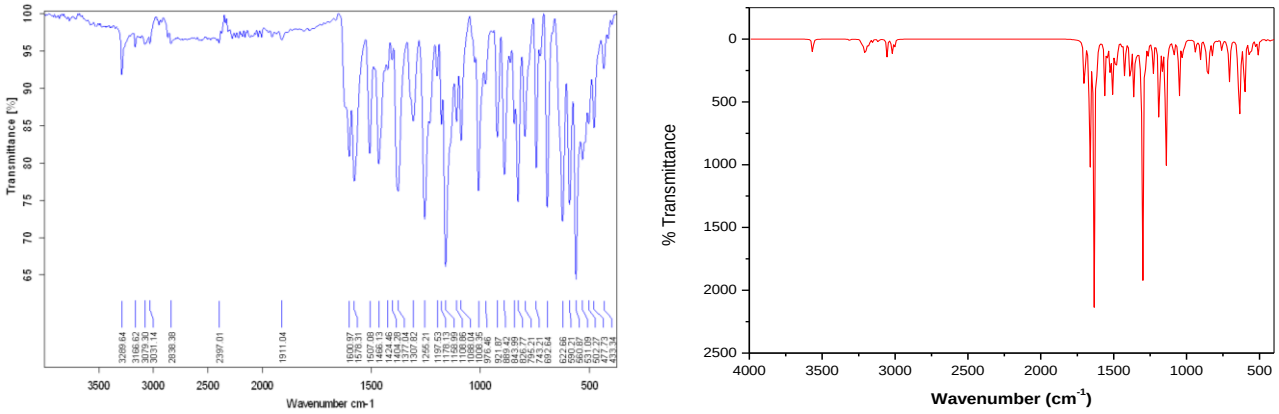

Fig. 2: Experimental (a) and simulated (b) FT-IR spectrum of L^1

Same for L^2, (C = N) imine group appears in at 1610 cm^{-1} absorption [43]. The (N-H)sulfamide stretching vibration band is observed at 3145 cm^{-1}[43]. The ῡ (C = N) oxazole ring band appears at 1593 cm^{-1} in the experimental spectra of the investigated compounds. In parallel, the absorption band that appeared at 927 cm^{-1} is attributed to the vibration (S-N) sulfonamide group [43]. The simulated and experimental IR spectra of *L^1* are represented in Fig. 2. All of the experimental and theoretical of the main vibration bands are summarized in Table 2.

Electronic absorption data

The electronic absorption spectra of L^1, and L^2 recorded in DMSO are respectively shown in Fig. (3) and Fig. (4). L^1 exhibits an intense band near 275 nm (36363 cm^{-1}) and a low-intensity band around 345 nm (28985 cm^{-1}). L^2 exhibits two absorption bands, the first one is observed around 36363 cm^{-1} (275 nm) and the second at 28901 cm^{-1} (346 nm). All theoretical TD-DFT and experimental wavelengths, the electronic transitions, the corresponding oscillator strength factors, and their contributions are given in Table 3. Consequently, the spectrums of two target new sulfonamides simulated at the PCM model showed a satisfactory correlation between the calculated and observed results.

^{1}H NMR spectra

^{1}H NMR spectra of both compounds were recorded in DMSO-d6 (Fig. 5). The theoretical (δTheo) and experimental (δExp) ^{1}H NMR chemical shifts of the investigated compounds are summarized in Table 4. The Gauge– Independent Atomic

Table 3: Theoretical TD-DFT and experimental electronic absorption spectrum of L^1 and L^2 compound

Electronic transitions	Contribution %	Energy (eV)	λ theo (nm)	λ exp (nm)	Oscillator strength (f)	$\bar{\upsilon}$ (cm^{-1})	ε ($cm^1L.mol^{-1}$)	Electronic transitions
Compound L^1								
1								
HOMO→LUMO	5.58%	3.665	338.28	345	1.1780	28985	62000	π → π*
HOMO-1→LUMO	90.77%							
2								
HOMO-5→LUMO	34.34%	4.535	273.34	275	0.0219	36363	43900	π → π*
HOMO-2→LUMO	41.85%							
HOMO-1→LUMO	9.36%							
HOMO→LUMO+3	6.05%							
HOMO→LUMO+5	4.04%							
Compound L^2								
1								
HOMO-10→LUMO	72.24%	2.832	437.65	458	0.0000	36363	82000	π→π*
HOMO-10→LUMO+1	18.88%							
HOMO-5→LUMO	5.87%							
HOMO-1→LUMO	14.30%							
HOMO-4→LUMO	2.38%							
HOMO-10→LUMO	3.55%							
2								
HOMO-7→LUMO	16.41%	3.567	347.57	346	0.0000	28901	11800	π → π*
HOMO-7→LUMO+1	3.67%							
HOMO-4→LUMO+4	2.87%							
HOMO-3→LUMO	4.97%							
HOMO-3→LUMO+1	3.01%							
HOMO-3→LUMO+2	2.11%							
HOMO→LUMO	5.90%							
HOMO→LUMO+1	35.40%							
HOMO→LUMO+4	2.47							
3								
HOMO-7→LUMO	25.45%	4.1415	299.37	275	0.0069	21834	196	n→π*
HOMO-4→LUMO	44.31%							
HOMO-3→LUMO	26.85%							
HOMO-2→LUMO	15.34%							
HOMO-5→LUMO	8.16%							

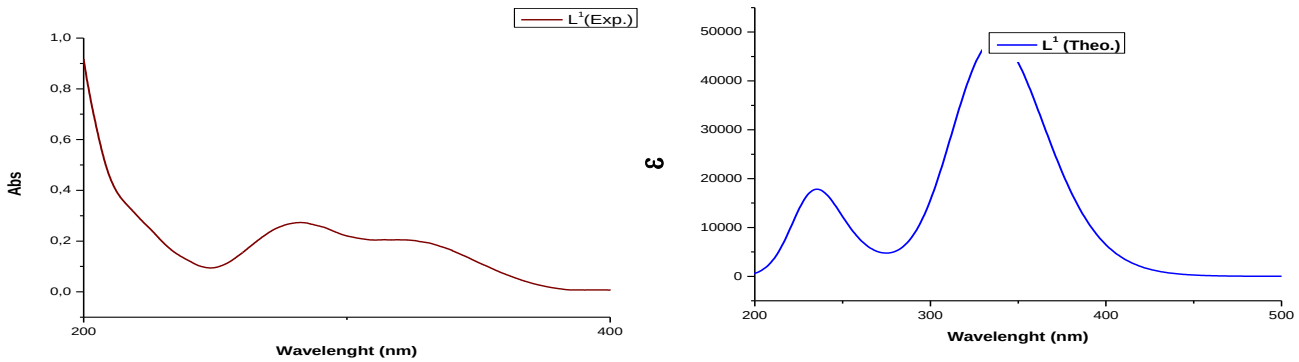

Fig. 3: Experimental (a) and theoretical (b) electronic spectra of L^1

Table 4: Main chemical shifts δ (ppm) of both L^1 and L^2 compounds.

Proton (multiplicity)	L^1		Proton (multiplicity)	L^2	
	δ_{Exp}	δ_{Theo}		δ_{Exp}	δ_{Theo}
H48(s) H49(s) H50(s)	2.31	2.48 2.55 2.51	H34(s) H35(s) H36(s)	2.29-2.34	2.47 2.52 2.49
H33(s)	6.08	7.40	H33(s)	6.08	6.72
H46(s)	11.39	6.2	H32(s)	10.94	6.35
H43(s)	8.53	8.62	H28(s)	9.94	8.53
H39(s) H40(s)	5.21	5.01 5.48	8H(t) Cycle (1+2)	6.78-8.02	7.34-8.82
13H (t) Cycle(1+2+3)	7.34-7.92	7.56-8.16	---	---	---

s: singlet, t: triplet

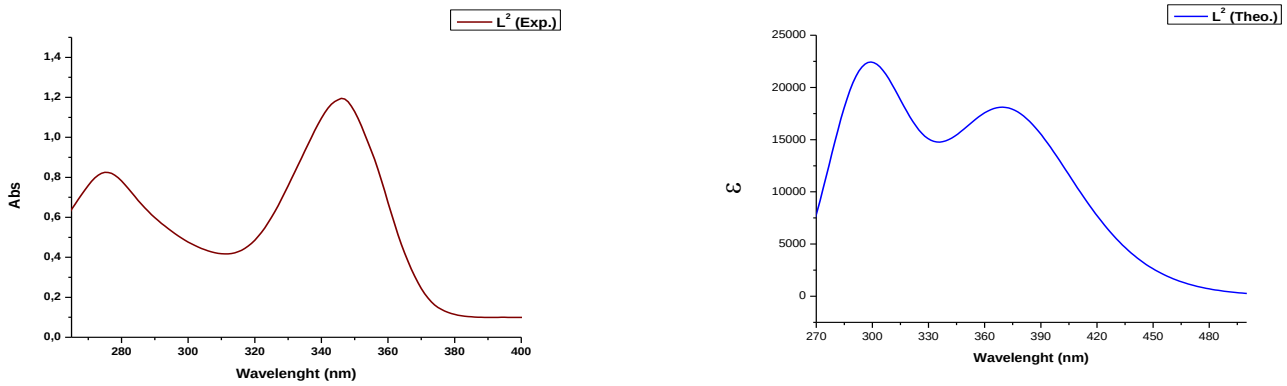

Fig. 4: Experimental (a) and theoretical (b) electronic spectra of L^2

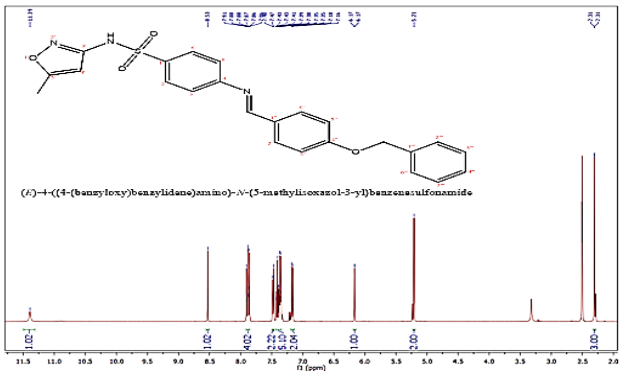

Fig. 5: ^{1}HNMR spectra of L^1

Orbital (GIAO) model [32] is attributed to calculating the absolute isotropic chemical shielding.

The spectra of both compounds revealed signals in the region [11.39-10.94] ppm and [8.53-9.94] ppm which are assigned to the (NH) group and of the proton C18 respectively. The signal that was recorded in the range of the [2.29-2.34] ppm of each ligand is attributed to the proton C6. The peaks of aromatic protons near the imine function which appear around [7.34-7.92] ppm in the compound L^1 have been shifted considerably in the L^2 and appear between [6.78-8.02] ppm. This important shift change is probably due to the replacement of the group phenyl of the compound L^1 by the group nitrogen dioxide which except an attractive effect. To compare the experimental and theoretical chemical shifts, a correlation graphic was presented in Fig. 6(a) for L^1 and Fig. 6(b) for L^2.

The correlation values for selected protons chemical shifts were found to be 0.9297 for L^1 and 0.9654 for L^2 (the protons ring and the Proton of N7H47 bond are not displayed for the correlation curve of L^1 also the protons rings and the proton of N7H32 are not displayed in Correlation curve of L^2) (Fig. 7); which reveals a satisfactory consistency between experimental and theoretical ^{1}H NMR data. From these results, we can conclude that the chosen DFT methods may predict experimental spectra with reasonable accuracy. The recorded carbon NMR spectrum (Fig. 8) shows that the number of signals displayed is consistent with the carbon number of the proposed structure. The spectrum shows a signal at 12.52 ppm of the CH3 group, another signal at 162.01 ppm

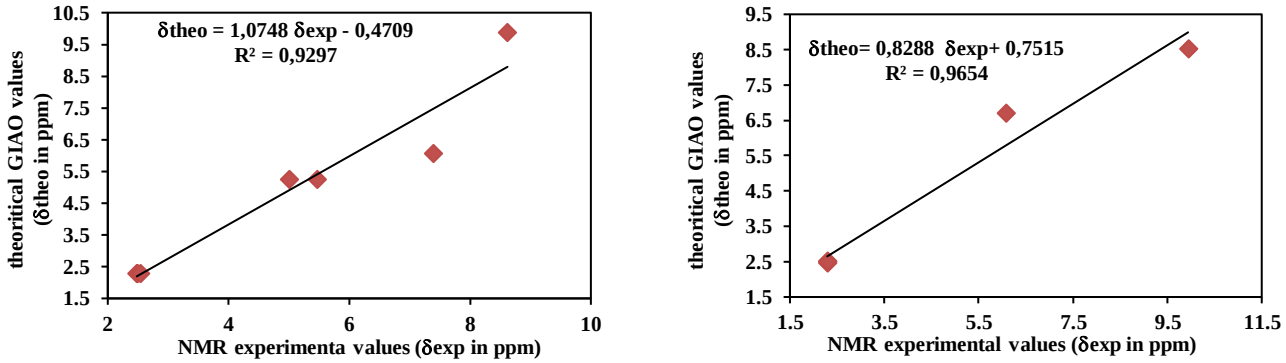

Fig. 6: (a) Protons chemical shifts correlation of L^1, (b) Protons chemical shifts correlation of L^2

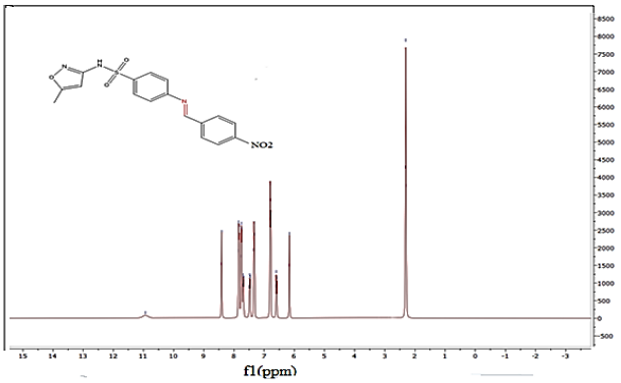

Fig. 7: ^{1}HNMR spectra of L^2

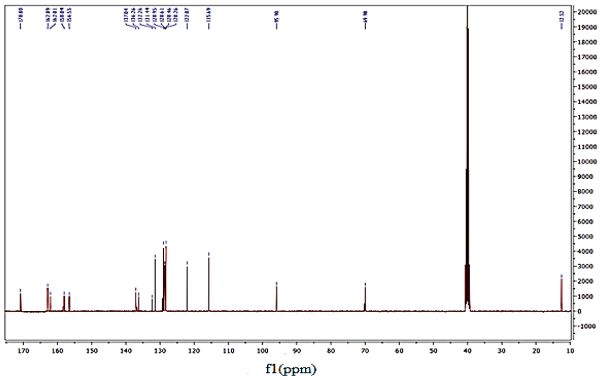

Fig. 8: ^{13}C NMR spectra of L^1

thus confirming the formation of a Schiff base, and a signal at 69.98 ppm attributed to the CH2 group. Aromatic carbons are observed at 115.69-170.80 ppm [44]. To elucidate the cis or trans isomerism, we carried out a 2D NMR analysis (HMBC). The latter revealed that hydrogen (H-C=N) shows a correlation with the C-3 and C-5 carbons, this confirms that hydrogen (H-C=N) and on the same side as the benzylidene group and therefore the isomerism is trans (Fig. 9).

THEORETICAL CALCULATIONS

Geometry optimization

The optimized structure of L^1 and L^2 at the DFT level is presented in Fig. 10. Bond lengths, valence angles, and dihedral angles for L^1 and L^2 are summarized in Table 5.

In the absence of L^1 and L^2 crystal structures, the optimized geometrical parameters of the Schiff base derivates are compared to their experimental values for various analogs [45]. In both structures, the higher bond length carried out with the use of the DFT method is in C9-S8. The C2-C3 bond for L^1 and L^2 is respectively 1.425 Å and 1.424 Å in oxazole rings. Then the 05-N4 bond for L^1 and L^2 is respectively 1.401 Å and 1.403 Å, which is similar to the experimental results reported in the literature [46]. In benzene rings, the Carbon-Carbon bond lengths vary in the range 1.393-1.407 Å. C-H bond lengths for methyl group in L^1 and L^2 are 1.091-1.094 Å. It is of note that the shorter DFT calculated bond length is obtained in N-H, this result justifies the electronegativity of the nitrogen atoms attached to hydrogen atoms. Then, the experimental values of N7-S8 bond lengths are in the range of 1.626–1.654 Å [44-46]. For L^2 is 1.232 Å. The C-H bond lengths are in the range of 1.076-1.094 Å. Finally, S=O bond lengths are 1.461 for L^1 and L^2 as agreed with the literature data [46,47]. The N17-C18-C19 valence angle is 123° and 122, 4°for L^1 and L^2 respectively. This difference is due to the difference in their environment. For the L^2 compound, the DFT degree O38-N37-O39 and O10-S8-O11 valence angles acquire values of 124.4 degrees and 122.9 degrees respectively. This result explains the difference in electronegativity between nitrogen and sulfur atoms. In parallel, the calculated bond angle C13-C14-N17 is equal to 117.9 degrees for L^1 and 122.9 degrees for L^2. The same situation is observed in the N17-C18- C19 bond

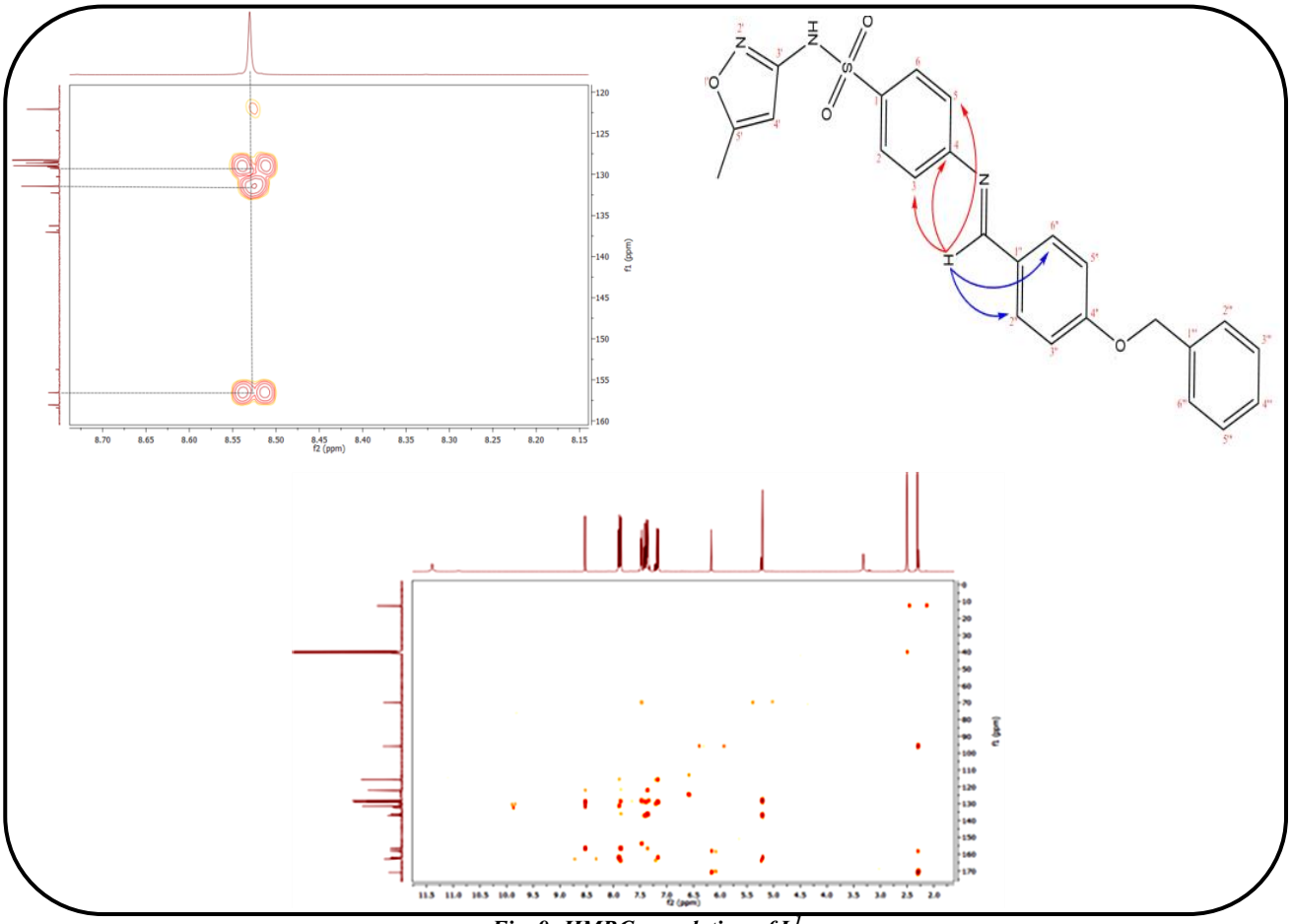

Fig. 9: HMBC correlation of L^1

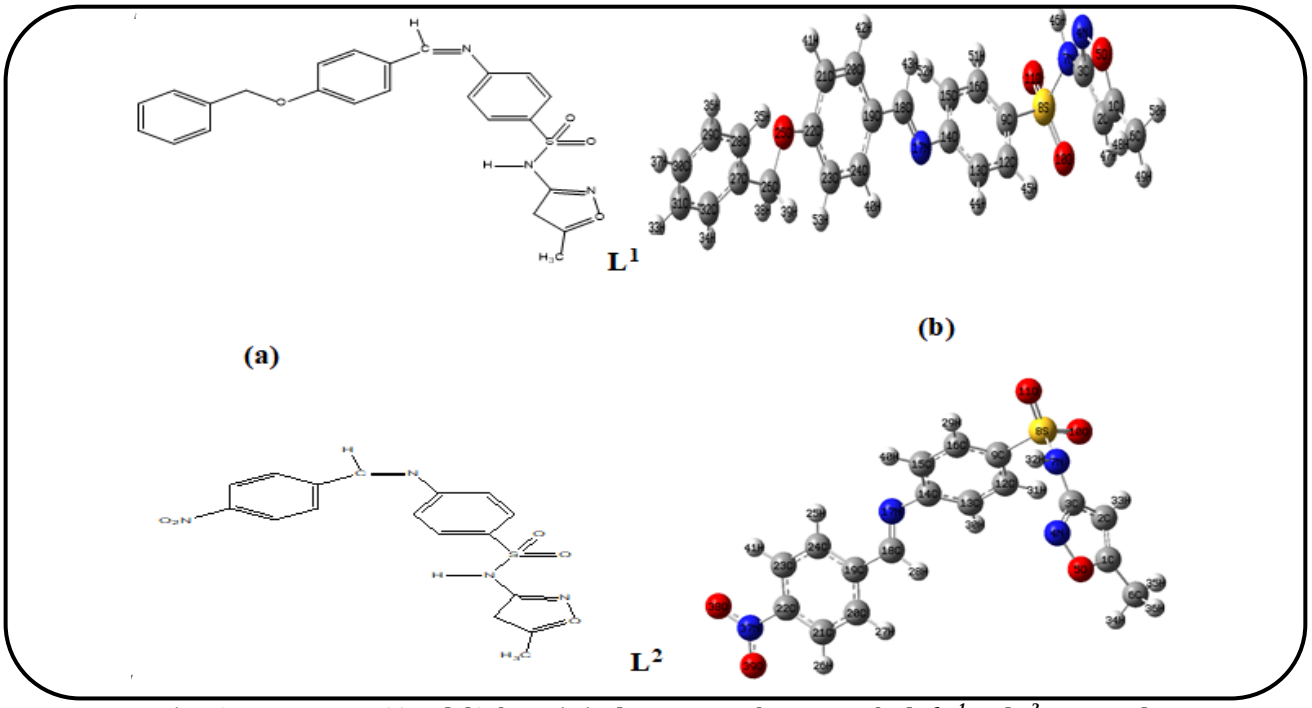

Fig. 10. 2D structures (a) and (b) the optimized structure at the DFT method of L^1 and L^2 compounds

Table 5: B3LYP/6-31G (d, p) computed structural parameters for L^1 and L^2. Bond lengths are in angstroms and angles in degrees

Parameters	L^1	Parameters	L^2	Experimental
	Bond distances		Bond distances	
C1-C2	1.362	C1-C2	1.363	1.377[d]
C1-C6	1.488	C1-C6	1.487	
C1-O5	1.352	C1-O5	1.354	
C2-C3	1.425	C2-C3	1.424	
O5-N4	1.401	O5-N4	1.403	1.409[a], 1.417[c]
C3-N7	1.399	C3-N7	1.402	
N7-H47	1.016	N7-H32	1.018	
N7-S8	1.707	N7-S8	1.703	1.653[a], 1.635[b], 1.626[b], 1.654[d]
S8-O10	1.461	S8-O10	1.465	1.434[a], 1.418[b], 1.427[c], 1.423[d]
S8-C9	1.787	S8-C9	1.784	1.731[a], 1.735[b], 1.768[c], 1756[d]
N17-C18	1.284	N17-C18	1.282	
C18-C19	1.459	C18-C19	1.469	
C19-C20	1.407	C19-C20	1.407	
C22-O25	1.358	C20-H27	1.083	
O25-C26	1.432	C22-N37	1.466	1.388[a], 1.398[b], 1.401[d]
C26-C27	1.508	N37-O38	1.232	
C26-H39	1.099	N37-O39	1.230	
C27-C28	1.400	C6-H36	1.094	
C6-H49	1.091	C2-H33	0.076	
C2-H33	0.077			
	Valence angles		Valence angles	
C1-C2-C3	103.2	C1-C2-C3	124.4	
C1-O5-N4	109.4	C1-O5-N4	118.6	
N4-C3-N7	118.9	N4-C3-N7	118.4	108.5[a]
C13-C12-H45	108.6	C13-C12-H31	119.4	118.2[a]
N7-S8-O11	105.9	N7-S8-O11	122.0	
C3-N7-H47	113.6	C3-N7-H32	117.6	
O10-S8-O11	122.8	O10-S8-O11	120.7	
S8-C9-C12	119.7	S8-C9-C12	121.0	120.08[a], 120.0[b], 119.9[d], 121.4[d]
C9-C12-C13	119.3	C9-C12-C13	107.8	
C13-C14-N17	117.8	C13-C14-N17	122.9	
N17-C18-C19	123.0	N17-C18-C19	122.4	112.1[a]
C19-C20-C21	121.0	C19-C20-C21	111.8	120.4[d]
C22-O25-C26	118.9	N27-C29-N30	118.7	
C27-C28-C29	120.3	C29-N32-O33	104.6	
O25-C26-C27	108.8	O33-C31-C30	109.8	
H36-C28-C27	119.3	O38-N37-O39	123.8	110.3[b]
	Torsion angles		Torsion angles	
C1-O5-N4-C3	-1.107	C1-O5-N4-C3	-1.070	
C3-C2-C1-O5	-0.312	C3-C2-C1-O5	-0.408	
C3-C2-C1-C6	179.61	C3-C2-C1-C6	179.83	

Continu Table 5: B3LYP/6-31G (d, p) computed structural parameters for L^1 and L^2. Bond lengths are in angstroms and angles in degrees

Parameters	L^1	Parameters	L^2	Experimental
	Torsion angles		Torsion angles	
C3-N7-S8-O10	179.71	C3-N7-S8-O10	179.50	
O5-N4-C3-N7	-175.67	O5-N4-C3-N7	-175.61	
O10-S8-C9-C12	159.35	O10-S8-C9-C12	156.77	
C12-C13-C14-N17	179.41	C12-C13-C14-N17	178.28	
N17-C18-C19-C24	-1.415	N17-C18-C19-C24	-0.350	
C24-C23-C22-O25	179.75	C-24-C23-C22-N37	179.97	
O25-C26-C27-C32	135.31	C23-C22-N37-O38	-179.97	
O25-C26-C27-C28	-46.70	C23-C22-N37-O39	0.05	
C28-C29-C30-C31	-0.378			

Experimental geometrical parameters for similar compounds found in the literature [a] Ref. [46] [b] Ref. [48] [c]Ref. [49] [d]Ref. [47]

Table 6: Global reactivity descriptors for L^1 and L^2 at the level DFT/6-31G (d, p)

Ligand	HOMO (eV)	LUMO (eV)	$\Delta E_{\lvert HOMO-LUMO \rvert}$ (eV)	I (eV)	A (eV)	μ (eV)	η (eV)	S (eV)	ω (eV)	Nu (eV)
L^1	-6.076	-1.913	4.164	7.379	-0.528	-3.953	3.959	0.126	1.973	-7.379
L^2	-6.698	-3.009	3.689	8.802	-1.047	-3.877	4.92 4	0.101	1.101	-8.802

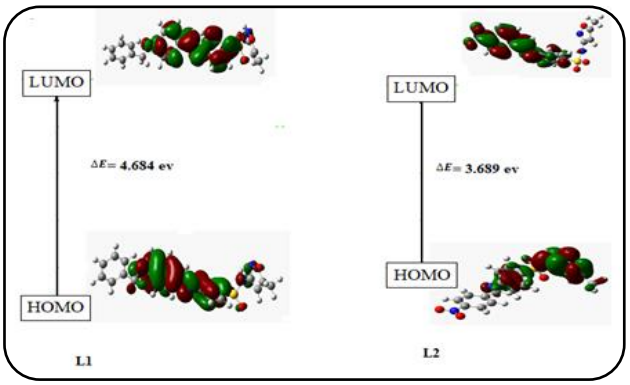

Fig. 11: Energy levels of the HOMO, LUMO, and energy band gap of L^1 and L^2.

angle where their values are respectively 123 degrees and 122.4 degrees in L^1 and L^2 compounds. These precedent results confirm the double bond character of particular azomethine function (N17=C18).

Frontier Molecular Orbitals

FMOs (Frontier molecular orbitals) are the most important orbitals in a molecule, HOMO and LUMO play very important roles in chemical stability and chemical reaction [23].

The HOMO (highest occupied molecular orbital) presents the energy which determines the capacity of a molecule to cede an electron (directly related to the ionization potential), and LUMO (lowest unoccupied molecular orbital) presents the energy which determines the ability to accept an electron (directly related to electron affinity) [48-50].

In many theoretical investigations, energies of HOMO and LUMO are popular quantum mechanical descriptors. It has been shown that these orbitals play a major role in governing many chemical reactions, and are also responsible for charge transfer [51]. The treatment of the frontier molecular orbitals, separately from the other orbitals, is based on the general principles governing the nature of chemical reactions. The concept of hard and soft nucleophiles and electrophiles has been also directly related to the relative energies of the HOMO and LUMO orbitals. Soft nucleophiles have a high energy HOMO [23].

The gap of énergy ΔE|HOMO-LUMO| is related to the biological activity of a molecule [40], the results of HOMO and LUMO energies and the HOMO–LUMO band gap of L^1 and L^2 are given in Table 6 and schematized in Fig. 11.

For compound L^1, the HOMO and LUMO are principally located on the two aromatic rings (except the benzyloxy moiety) and the amine group and the two oxygens of the sulfonamide function, in contrary for L^2, the HOMO is located on the oxazole's ring, the LUMO distribution is located in benzene ring and NO2 group. The values of HOMO-LUMO gap energy are respectively equal to 4.164 and 3.689 eV (1Hartree=27,2114eV)for L^1, and L^2. The lowering in the HOMO-LUMO energy gap explains the potential for charge transfer interactions to take place within the molecule, which may be responsible for the bioactivity of the molecule [52-55]. According to the energy gap, L^2 seems to be more reactive than L^1.

Global chemical reactivity

To explain the reactivity and the biological activities of the synthesized compounds L^1 and L^2 [56], the global electronic descriptors were calculated (see Table 6). The values of m, h, S, w, and Nu were calculated using the Eqs. (1) to (5) respectively by DFT methods such us (m) represents the electronic chemical potential, (h) the absolute hardness, (S) the global softness, (w) the global electrophilicity and (Nu) the global nucleophilicity [51,52].

$$\mu = -\frac{1}{2}(I + A) = -\chi \quad (1)$$

$$\eta = \frac{1}{2}(I - A) \quad (2)$$

$$S = \frac{1}{2\eta} \quad (3)$$

$$\omega = \frac{\mu^2}{2\eta} \quad (4)$$

$$Nu = - I \quad (5)$$

The ionization potential (I) and electron affinity (A) of the molecule were calculated by the Eqs. (6) and (7) respectively:

$$I = E\,(N\text{-}1) - E\,(N) \quad (6)$$

$$A = E\,(N+1) - E\,(N) \quad (7)$$

Where E(N) and E (N - 1) are the total ground-state energies in the neutral N and singly charged (N -1) configure. urations, respectively.

According to these parameters, the chemical reactivity varies with the structure of molecules. The chemical hardness value of compound L^1 is lesser than the chemical hardness of L^2 implying that the charge transfer process is more predominant in L^1 compared to L^2. Thus, compound L^1 is found to be more reactive than L^2. Compound L^1 possesses a higher electronegativity value than L^2 so; it is the best electron acceptor. The values of ω for compounds L^1 indicate that L^1 has a high value of electrophilicity index which, shows that it is a stronger electrophile than L^2. Also, the nucleophilicity index Nu shows that L^1 is better nucleophilic than L^2. From these results, L^1 appears more reactive than L^2. The dipole moment (m in Debye) is an electronic parameter that results from the non-uniform distribution of charges on the various atoms in molecules, for L^1 (7.9 Debye) and L^2 (5.07 Debye) given in Table 7.

NBO charges and molecular electrostatic potential analysis

In quantum chemistry, a Natural Bond Orbital (NBO) is used to understand the site of electrophilic and nucleophilic attack [51]. NBO charges represent a calculated bonding orbital with maximum electron density. According to the calculated atomic charges represented in Table 7 for L^1 S8 sulfur atom has a higher positive charge (+2.361 e) compared to other atoms which is due to the attaching of three electronegative atoms: two oxygèn atoms and one azote atom which are O10 (-0.960 e), O11 (-0.957 e) and N7 (-0.891 e). Likewise, for L^2, sulfur S8 represents a higher positive charge (+2. 359 e) for the same reason as the L^1 compound and O10, O11 atoms have the largest négative charge (-0.962 e), (-0.958 e) respectively.

The electrostatic potential generated by a molecule's electrons and nuclei in the space around it is a very useful property for analyzing and predicting molecular reactive behavior [55,57]. The molecular electrostatic potential surface (MEP) collects a wealth of information, including molecules' dipole moments, molecular shape, and electrostatic potential distribution. It provides an illustration method for understanding a molecule's relative polarity. The molecular electrostatic potential can be used to identify the molecular targets for electrophilic and nucleophilic assaults. Different colors are used to represent the various electrostatic potential levels at the surface. The MEP color scheme represents the electron-rich and electron-poor regions, which means that the intermediate colors of yellow and light blue are respectively correspond to the slightly electron-loaded region and the slightly electron-poor region. Blue is associated with the electron-deficient or partially positive charge, while red is associated with the rich sites in electrons [23].

The SCF (Self Consistent Field) of surface electron density traced with MEP of the compound is shown in Fig. 12. For L^1 the total electron density varies between two extreme limits:-5,362.10^{-2} a.u to +5.362.10^{-2} a.u. The most electron-deficient region is around the aromatic rings including between +0,168.10^{-2} a.u and +2,744.10^{-2} a.u.For L^2 the total electron density varies between two extreme limits:-8,944.10^{-2} a.u to +8.944.10^{-2} a.u the negative regions are mainly localized on the oxygen atoms, corresponding to -4.238.10^{-2} a.u, and -1.449 .10^{-2} a.u interval. Then, the electron density reveals the polarity of the molecule. The MEP indicates the electron-poor region of the Schiff bases. Consequently, The NBO charges are

Table 7: NBO atomic charges (e) and dipole moment (in Debye) of the L^1 and L^2.

L^1				L^2			
Atom	NBO charge	Atom	NBO charge	Atom	NBO charge	Atom	NBO charge
C1	0.372	C28	-0.230	C1	0.374	H28	0.213
C2	-0.389	C29	-0.233	C2	-0.390	H29	0.274
C3	0.318	C30	-0.243	C3	0.317	H30	0.264
N4	-0.209	C31	-0.238	N4	-0.207	H31	0.275
O5	-0.326	C32	-0.233	O5	-0.326	H32	0.468
C6	-0.745	H33	0.283	C6	-0.745	H33	0.284
N7	-0.891	H34	0.250	N7	-0.888	H34	0.270
S8	2.361	H35	0.248	S8	2.359	H35	0.270
C9	-0.364	H36	0.251	C9	0.249	H36	0.270
O10	-0.960	H37	0.249	O10	-0.962	N37	0.519
O11	-0.957	H38	0.249	O11	-0.958	O38	-0.401
C12	-0.214	H39	0.232	C12	-0.207	O39	-0.401
C13	-0.234	H40	0.236	C13	-0.250	H40	0.260
C14	0.164	H41	0.245	C14	-0.156	H41	0.281
C15	-0.259	H42	0.259	C15	-0.226		
C16	-0.207	H43	0.260	C16	-0.209		
N17	-0.479	H44	0.204	N17	-0.444		
C18	0.130	H45	0.262	C18	0.124		
C19	-0.152	H46	0.271	C19	-0.082		
C20	-0.173	H47	0.461	C20	-0.197		
C21	-0.321	H48	0.269	C21	-0.208		
C22	0.347	H49	0.269	C22	0.067		
C23	-0.285	H50	0.269	C23	-0.211		
C24	-0.190	H51	0.272	C24	-0.190		
O25	-0.525	H52	0.261	H25	0.271		
C26	-0.124	H53	0.260	H26	0.282		
C27	-0.070			H27	0.265		
Dipole Moment		7.9				5.05	

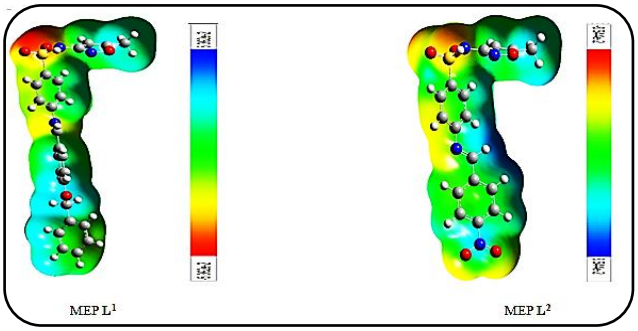

Fig. 12: The total electron density surfaces of L^1 and L^2

in agreement with the total electron density surfaces for the two new synthesized Schiff bases.

Antibacterial Activity

The antimicrobial activity of the sulfonamide derivatives L^1, and L^2 was evaluated against four bacterial strains: *Escherichia coli*, *Pseudomonas aeruginosa* (Gram-negative), *Staphylococcus aureus*, *Streptococcus sp* (Gram-positive). Gentamicin pure drug was used as a reference [12,58]. The *in vitro* antibacterial results show that the synthesized compounds exhibit notable antiproliferative activity against *Escherichia coli* and Staphylococcus aureus However, no activity is observed against *Pseudomonas aeruginosa*. The comparative results are displayed in Fig. 13. Remarkably, the tested compounds showed a high bacteriostatic effect against

Table 8: Zone of inhibition (mm) of (L^1, L^1) and reference drug.

compounds	Bacterial strains				Fungal strains
	E. coli	P.aeruginosa	S. aureus	Streptococcus sp	C.albicans
L^1	60	-	36	20	13
L^2	60	-	32	15	-
Gentamicine	60	20	25	20	-
Ketoconazole	-	-	-	-	35

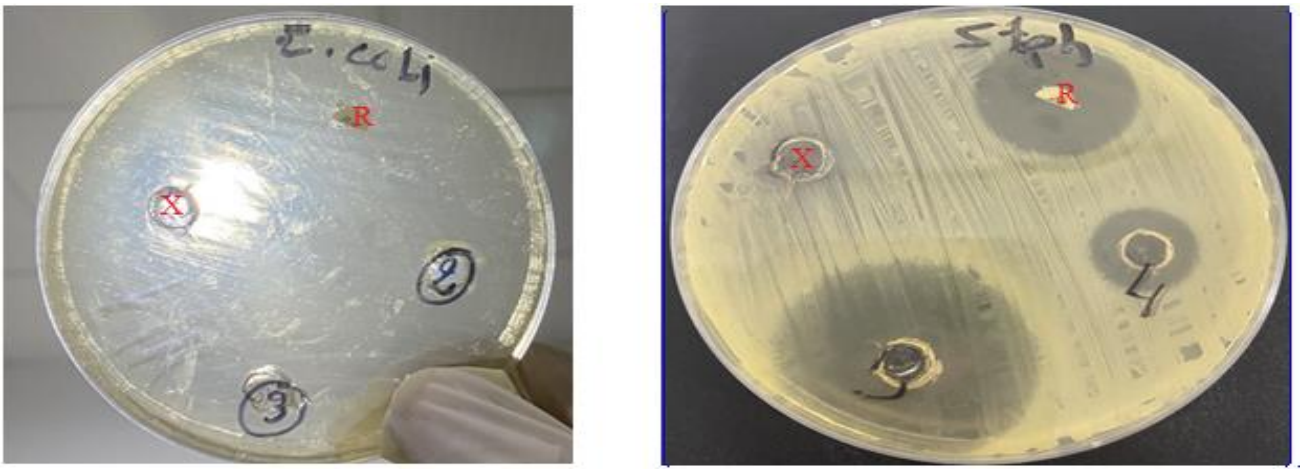

Fig. 13: In vitro sensitivity with E. coli to 3: L^1, 2: L^2 and with S.aureus à 5:L^1, 4 :L^2 ,R: standard drug, X: negative control

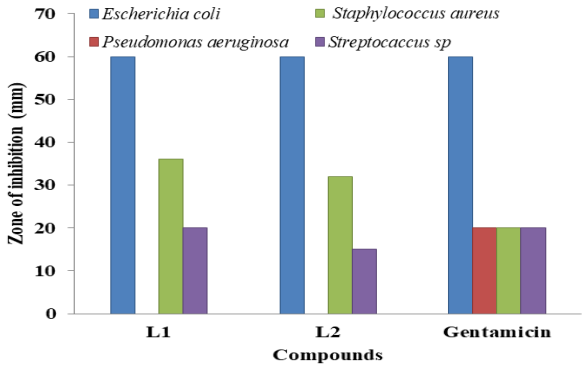

Fig. 14: antimicrobial activity of ligands L^1 and L^2.

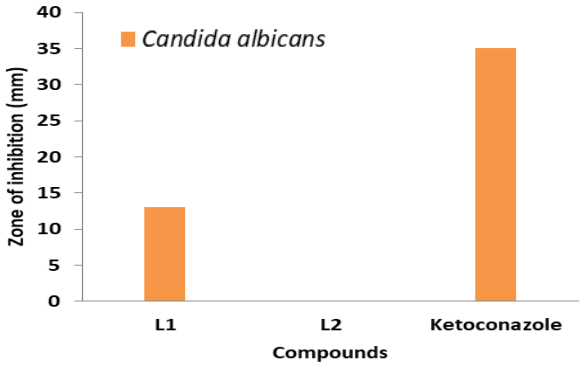

Fig. 15: antifungal activity of compounds L^1 and L^2.

both Gram-positive and Gram-negative bacteria with a zone of inhibition diameters in the 20-60 mm range. Moreover, in comparison to the reference, the tested compounds displayed similar antibacterial activity to the Gentamicin drug which confirms their potential as antibacterial agents (see Table 8).

The poor activity against *Pseudomonas aeruginosa* is probably due to the composition of the membrane cell of the bacteria. Indeed, the phospholipid species found in the cell membrane prevent the diffusion of active substances into the cytoplasm, which gives it resistance to most biocidal agents [40, 54]. Also, it is noted that *Pseudomonas aeruginosa* exhibits fast adaptation to changes in environmental conditions which confer high antibiotic resistance [57]. The reference has no antimicrobial activity (see Fig. 13).

Antifungal activity

The antifungal potential of the Schiff bases was evaluated against the *Candida albicans* strain. Ketoconazole was used as a reference drug [12,58]. The comparative results as shown in Figs. 14 and 15 indicate that the newly synthesized compounds display weak antiproliferative

Table 9: Predicted pharmacokinetic and drug-likeness properties of the compounds L^1, L^2, and sulfamethoxazole as standard drugs with SwissADME and admetSAR online servers.

Compound	BBB	HIA	$CaCo_2$	Molecular Weight (g/mol)	TPSA (Å²)	HBD	HBA	Rotatabl Bonds	Log p	Lipinski's violation
L^1	0.7865+	0.9970+	0.5709-	447.51	101.17	1	6	8	3.26	0
L^2	0.8092+	0.9891+	0.5455-	386.38	138.76	1	7	6	1.66	0
SMX	0.9382+	1.0000+	0.5346-	253.28	106.60	2	4	3	1.09	0

Table 10: Toxicity estimation of the synthesized compounds.

Compound	Carcinogenicity	Ames Toxicity	Acute oral toxicity (mg/L
L^1	Non-carcinogen	Non-toxic	III**
L^2	Non-carcinogen	Non-toxic	III**
SMX	Non-carcinogen	Non-toxic	IV*

***LD50 greater than 500m/kg, slightly toxic , ** LD50 greater than 5000m/kg, nontoxic**

activity against the tested strain. Indeed, L^1 showed moderate activity with a zone of inhibition around 13 mm while L^2 displayed no antifungal properties. The poor antifungal properties of the Schiff bases could be explained by the fact that sulfamethoxazole, our starting material, has no significant antifungal properties. Indeed, the sulfa drug is best known for its antibacterial properties in synergy with the Trimetoprim drug [59]. Additionally, the chemical composition of the fungi cell walls is different from the one of bacteria [60]. This could explain the fact that the synthesized compounds displayed high antibacterial properties and very low antifungal activity.

ADMET and drug-likeness analysis

The ADME and toxicity results of the ligands are presented in Tables 9 and 10 respectively, the calculation is performed by SwissADM (http://www.swissadme.ch) [35] and dmetSAR (http://lmmd.ecust.edu.cn/admetsar2) [36] servers. Results show that the sulfonamide compounds L^1, and L^2 don't penetrate through the blood-brain barrier (BBB), which indicates that the compounds could be innocuous to the CNS (central nervous system) and they exhibit a good intestinal absorption, comparable to standard sulfamethoxazole (SMX), This suggests that the compounds are well absorbed by the gastrointestinal tract and, as a result, could be effective drugs. In the same way, Lipinski's rule [37], known as the rule of five evaluates the molecules by four physicochemical properties: molecular weight should be less than 500, hydrogen bond donors and acceptors should be respectively $\leq$ 5 donors and $\leq$10 acceptors, and the lipophilicity LogP $\leq$ 5. All the compounds passed the test since non-violation (or only one) of this rule was detected. The polar surface area (PSA) and the number of rotatable bonds are linked with oral bioavailability, those parameters should be equal to or less than 140 Å² cutoff for PSA and 10 or fewer rotatable bonds, they are described by Veber's rule [38]. This rule applies to all of the compounds. Additionally, the estimated toxicity indicates that the compounds are non-mutagen (non-AMES toxic), non-carcinogen, and non-oral toxic. Toxicity results are depicted in Table 10**.** The ADMET and drug-likeness of the newly synthesized sulfonamide derivative compounds present a promising result which makes them important antimicrobial and antifungal drug candidates.

Molecular docking study

Molecular docking is an intriguing method for investigating the interaction between small molecules and proteins, which could explain the antimicrobial activity of our newly synthesized compounds. Molecular docking simulations were run on *Escherichia coli* bacterial strains, The crystal structures of the bacterium's dihydropteroate synthase enzyme (DHPS), the target enzyme of sulfonamides, were obtained from the Protein Data Bank (PDB) Website (*E. coli*, PDB: 1AJ0) [61,62]. AutoDock Tools was used to compute Gasteiger charges. The binding site and active amino acids of the enzymes are defined using the reference [61] and Biovia Discovery Studio 4.5 by selecting co-crystallized ligands. The redocking of the native compounds of the employed proteins into their respective binding sites served to validate the docking protocol, and the RMSD values obtained were less than 2 Å. The best poses among the twenty generated conformations

Table 11: Energies of interactions, hydrogen bonds, and hydrophobic interactions between the synthesized compound (L^1, L^2) and E.coli (1AJ0) receptor.

	Interactions				
Compounds	H-bond	Pi-alkyl	alkyl	Other interactions	Score (Kcal /mol)
L^1	O ARG^{63} NH2 , N ARG^{63} OH O THR^{257} H	LYS^{121} PRO^{64} ALA^{151}	-	PRO^{64} (pi-lone pair) HIS^{257} (pi-sulfur)	-10,55
L^2	O ASN22 NH O ARG255 NH O HIS257 NH O ARG63 NH2 NH THR147 O, N THR147OH O GLY191 NH	PRO^{64}	PHE^{190} MET^{141} PRO^{145}	-	-11,11
Sulfamethoxazole	N GLY^{191} NH, NH GLY^{189} O NH2 GLN^{142} O			ALA^{151}	-7,46

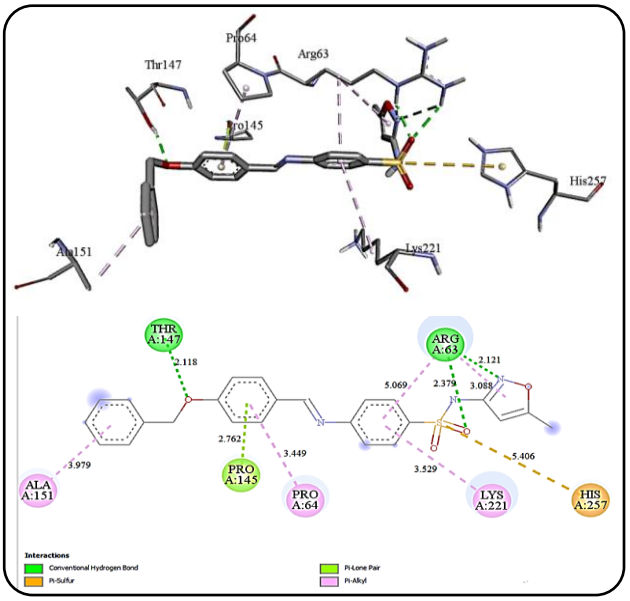

Fig. 16: 3D and 2D docking conformation compound 1-1AJ0 complex.

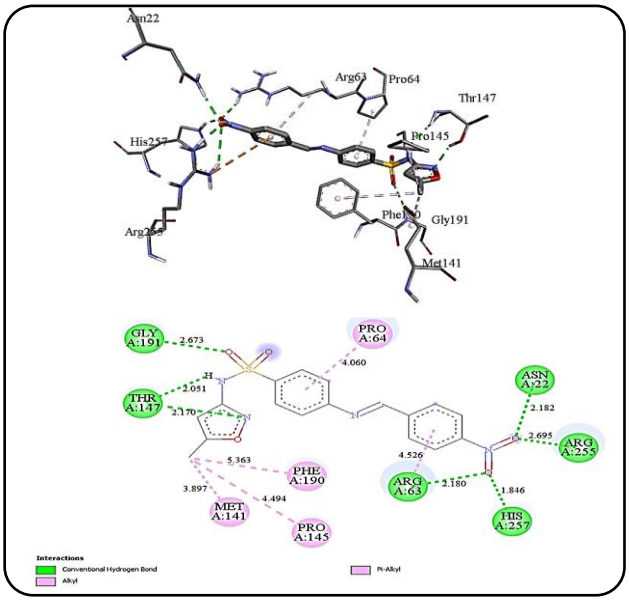

Fig. 17: 3D and 2D docking conformation compound 2-1AJ0 complex

were chosen based on binding affinity and hydrogen bond interactions. The 3D and 2D binding poses of the compound are represented in Figs. 16 and 17 and all the interactions between the protein and the studied compound are summarized in Table 11 [63-66].

The binding affinity of the compound L^1 DHPS (*E. coli*) and compound L^2 DHPS (*E. coli*) complex are -10.55kcal/mol and -11.11kcal/mol, respectively. These values indicate that the newly synthesized compounds interact more strongly than the sulfamethoxazole with the receptor (-7.46 kcal/mol).

The compound L^1 binds to the DHPS of *E. coli* through three hydrogen bonds, two with ARG63 one with the oxygen atom of the -SO2 group, and the second with the nitrogen atom of the oxazolic ring with 2.379 Å and 2.121 Å bond length respectively. In addition, the hydrogen atom of the benzyloxilic group interacts with THR147 with 2.118 Å bond distances. While the three benzene rings exhibit hydrophobic pi-alkyl interactions, with (ARG63, PRO64, LYS221, and ALA151), respectively and the oxazole ring interacts with ARG63. We also note a pi-sulfur interaction with HIS257 amino-acid and pi-lone pair PRO145 (d=2.762Å). The ligand L^2 exhibits seven hydrogen bonds with the macromolecule, two oxygens of the -NO2 group form four hydrogen bonds of ASN22, ARG255, HIS257, and ARG63 residues, respectively and two hydrogen bonds with THR147 amino acid with the sulfonamides (d=2.051Å) and oxazoles (d=2.170Å)

nitrogen, while one the oxygen of the –SO2 group interact with GLY191 amino acid (d=2.673Å). On the other hand, sulfamethoxazole as standard drug forms less hydrophobic interactions than the ligands, this is consistent with the predicted logP values which predict the sulfamethoxazole (logP=0.90) as more hydrophilic than the compound L^1 (logP=3.26) and the compound L^2 (logP=1.66) Table 9. As a result, the synthesized compounds may act as inhibitors of *E. coli* DHPS enzymes, which correlate with in vitro antibacterial activity.

CONCLUSIONS

Two new Schiff base derivatives were synthesized and characterized, by FT-IR, 1H NMR, 13C-NMR, Mass spectroscopy (SM), UV–Visible spectroscopy. The geometries of the novel compounds were optimized using the DFT/6-31G (d, p). The frontier molecular orbitals FMOs, and the global reactivity descriptors showed a good correlation between experimental and theoretical results. The antimicrobial activity of the tested compounds shows a significant activity against tested strains, especially on *Escherichia coli*. The L^1 Schiff base shows better antimicrobial activity than L^2 against tested bacterial and fungal strains. In the theoretical study and based on chemical reactivity descriptors (m, h, S, w, and Nu), L^1 appears more reactive than L^2 which is in agreement with the experimental study. Molecular Docking results show that the synthesized compounds are stabilized by hydrogen bonds and hydrophobic interactions with acceptor sites of the receptors, which support their antimicrobial activity. The ADMET study was carried out to predict the pharmacokinetic parameters and toxicity of compounds. A good drug-link behavior and a non-toxic nature were observed. The obtained results show that the newly synthesized compounds can be considered promising antimicrobial agents.

Received: Jun. 29, 2023; Accepted: Aug. 21, 2023

REFERENCES

[1] Sengupta S., Chattopadhyay M.K., Grossart H.-P., The Multifaceted Roles of Antibiotics and Antibiotic Resistance in Nature, *Frontiers in microbiology*, **4:** 47 (2013).

[2] Nazirkar B., Mandewale M., Yamgar R., Synthesis, Characterization and Antibacterial Activity of Cu (II) and Zn (II) Complexes of 5-Aminobenzofuran-2-Carboxylate Schiff base Ligands, *Journal of Taibah University for Science*, **13(1):** 440–449 (2019).

[3] Naaz F., Srivastava R., Singh A., Singh N., Verma R., Singh V.K., Singh R.K., Molecular Modeling, Synthesis, Antibacterial and Cytotoxicity Evaluation of Sulfonamide Derivatives of Benzimidazole, Indazole, Benzothiazole and Thiazole, *Bioorganic & Medicinal Chemistry*, **26(12):** 3414–3428 (2018).

[4] Manjunatha M., Naik V.H., Kulkarni A.D., Patil S.A., DNA Cleavage, Antimicrobial, Anti-Inflammatory Anthelmintic Activities, and Spectroscopic Studies of Co (II), Ni (II), and Cu (II) Complexes of Biologically Potential Coumarin Schiff Bases, *Journal of Coordination Chemistr*, **64(24):** 4264–4275 (2011).

[5] Mosalanezhad F., Asadzadeh A., Ghanbariasad A., Naderpoor M., Bordbar R., Ghavamizadeh M., Zolghadri S., The Evaluation of the Anti-Histone Deacetylase, Antibacterial, Antioxidant and Cytotoxic Activities of Synthetic N,N´-Ethylenebis (α Methylsalicylideneiminate) Schiff Base Derivatives, *Iran. J. Chem. Chem. Eng.*, **41(6):** 1856–1869 (2022).

[6] Lai C.-C., Chen S.-Y., Ko W.-C., Hsueh P.-R., Increased Antimicrobial Resistance during the COVID-19 Pandemic, *International Journal of Antimicrobial Agents*, **57(4):** 106324 (2021).

[7] Lucien M.A.B., Canarie M.F., Kilgore P.E., Jean-Denis G., Fénélon N., Pierre M., Cerpa M., Joseph G.A., Maki G., Zervos M.J., Dely P., Boncy J., Sati H., Rio A.D., Ramon-Pardo P., Antibiotics and Antimicrobial Resistance in the COVID-19 Era: Perspective from Resource-Limited Settings, *International journal of infectious diseases*, **104:** 250–254 (2021).

[8] Rodríguez-Baño J., Rossolini G.M., Schultsz C., Tacconelli E., Murthy S., Ohmagari N., Holmes A., Bachmann T., Goossens H., Canton R., Roberts A.P., Henriques-Normark B., Clancy C.J., Huttner B., Fagerstedt P., Lahiri S., Kaushic C., Hoffman S.J., Warren M., Zoubiane G., Essack S., Laxminarayan R., Plant L., Antimicrobial Resistance Research in a Post-Pandemic World: Insights on Antimicrobial Resistance Research in the COVID-19 Pandemic, *J. Glob. Antimicrobial Resistance*, **25:** 5–7 (2021).

[9] Lal J., Gupta S.K., Thavaselvam D., Agarwal D.D., Biological Activity, Design, Synthesis and Structure Activity Relationship of some Novel Derivatives of Curcumin Containing Sulfonamides, *European Journal of Medicinal Chemistry*, **64:** 579–588 (2013).

[10] Shin Y.S., Lee J.Y., Noh S., Kwak Y., Jeon S., Kwon S., Jin Y., Jang M.S., Kim S., Song J.H., Kim H.R., Park C.M., Discovery of Cyclic Sulfonamide Derivatives as Potent Inhibitors of SARS-CoV-2, *Bioorganic & Medicinal Chemistry Letters*, **31:** 127667 (2021).

[11] Bhat A.R., Dongre R.S., Patil R.C., Hassan S., et al, SARS-CoV-2 and Diabetes Mellitus (DM): A Comprehensive Review, *Inventum Biologicum: An International Journal of Biological Research*, **2(2):** 87–93 (2022).

[12] Hassan S.A., Aziz D.M., et al, Synthesis of New Series Bis-3-Chloro-β-Lactam Derivatives from Symmetrical Bis-Schiff Bases as Effective Antimicrobial Agents with Molecular Docking Studies, *Sci. J. Uni. Zakho*, 9 **(3):** 128–137 (2021).

[13] Aziz D.M., Hassan S.A., Hamad O.Q., Azo-Azomethine Complex Activity and Sensor Potential Toward Ca (II) Ion in Life Samples: the Spectroscopic and Morphological Studies, *Journal of Molecular Structure*, **1293:** 136204 (2023).

[14] Muhammed Aziz D., et al., New Azo-Azomethine Derivatives: Synthesis, Characterization, Computational, Solvatochromic UV–Vis Absorption and Antibacterial Studies, *Journal of Molecular Structure*, **1284:** 135451 (2023).

[15] Przybylski P., Huczynski A., Pyta K., Brzezinski B., Bartl F., Biological Properties of Schiff Bases and Azo Derivatives of Phenols, *Current Organic Chemistry*, **13(2):** 124–148 (2009).

[16] Pandeya S.N., Sriram D., Nath G., DeClercq E., Synthesis, Antibacterial, Antifungal and Anti-HIV Activities of Schiff and Mannich bases Derived from Isatin Derivatives and N-[4-(4'-Chlorophenyl)Thiazol-2-yl] Thiosemicarbazide, *European Journal of Pharmaceutical Sciences*, **9(1):** 25–31 (1999).

[17] Gümrükçü G., Karaoğlan G.K., Erdoğmuş A., Gül A., Avcıata U., A Novel Phthalocyanine Conjugated with four Salicylideneimino Complexes: Photophysics and Fluorescence Quenching Studies, *Dyes and Pigments*, **95(2):** 280–289 (2012).

[18] Lorcy D., Bellec N., Fourmigué M., Avarvari N., Tetrathiafulvalene-based Group XV Ligands: Synthesis, Coordination Chemistry and Radical Cation Salts, *Coordination Chemistry Reviews*, **253(9):** 1398–1438 (2009).

[19] Zoubi W.A., Biological Activities of Schiff Bases and Their Complexes: A Review of Recent Works, *International Journal of Organic Chemistry*, **3(3):** 73–95 (2013).

[20] Hassan S.A., et al., Design and Synthesis of Oxazepine Derivatives from Sulfonamide Schiff bases as Antimicrobial and Antioxidant agents with low Cytoxicity and Hemolytic Prospective, *Journal of Molecular Structure*, **1292:** 136121(2023).

[21] Hassan S.A., et al., In Vitro and in Vivo Evaluation of the Antimicrobial, Antioxidant, Cytotoxic, Hemolytic Activities and in Silico POM/DFT/DNA-Binding and Pharmacokinetic Analyses of New Sulfonamide Bearing Thiazolidin-4-Ones, *Journal of Biomolecular Structure and Dynamics*, 1-17 (2023).

[22] Hassan, S. A., et al, Synthesis, Spectroscopic study and Biological activity of some New Heterocyclic compounds derived from Sulfadiazine, *Zanco Journal of Pure and Applied Sciences*, **31(6):** 92-109 (2019).

[23] Hassan S.A., Aziz D.M., et al, An Efficient One-Pot Three-Component Synthesis, Molecular Docking, ADME and DFT Predictions of New Series Thiazolidin-4-One Derivatives Bearing a Sulfonamide Moiety as Potential Antimicrobial and Antioxidant Agents, *Egyptian Journal of Chemistry*, **65(8):** 133–146 (2022).

[24] Ela M.A., El-Shaer N., Ghanem N., Antimicrobial Evaluation and Chromatographic Analysis of some Essential and Fixed Oils, *Die Pharmazie*, **51(12):** 993–994 (1996).

[25] Frisch M.J., Trucks G.W., Schlegel H.B., Scuseria G.E., Robb M.A., Cheeseman J.R., Scalmani G., Barone V., Mennucci B., Petersson G.A., Nakatsuji H., Caricato M., Li X., Hratchian H.P., Izmaylov A.F., Bloino J., Zheng G., Sonnenberg J.L., Hada M., Ehara M., Toyota K., Fukuda R., Hasegawa J., Ishida M., Nakajima T., Honda Y., Kitao O., Nakai H., Vreven T., Montgomery J.A. Jr., Peralta J.E., Ogliaro F., Bearpark M., Heyd J.J., Brothers E., Kudin K.N., Staroverov V.N., Kobayashi R., Normand J., Raghavachari K., Rendell A., Burant J.C.,

Iyengar S.S., Tomasi J., Cossi M., Rega N., Millam J.M., Klene M., Knox J.E., Cross J.B., Bakken V., Adamo C., Jaramillo J., Gomperts R., Stratmann R.E., Yazyev O., Austin A.J., Cammi R., Pomelli C., Ochterski J.W., Martin R.L., Morokuma K., Zakrzewski V.G., Voth G.A., Salvador P., Dannenberg J.J., Dapprich S., Daniels A.D., Farkas O., Foresman J.B., Ortiz J.V., Cioslowski J., Fox D.J., Gaussian 09, Revision D.01, Gaussian, Inc., Wallingford, CT, (2009).

[26] Becke A.D., Density-Functional Exchange-Energy Approximation with Correct Asymptotic Behavior, *Physical Review A*, **38(6):** 3098–3100 (1988).

[27] Becke A.D., A New Mixing of Hartree–Fock and local Density-Functional Theories, *Journal of Chemical Physics*, **98(2):** 1372–1377 (1993).

[28] Becke A.D., Density-Functional Thermochemistry. III. The Role of Exact Exchange, *Journal of Chemical Physics*, **98(7):** 5648–5652 (1993).

[29] Lee C., Yang W., Parr R.G., Development of the Colle-Salvetti Correlation-Energy Formula into a Functional of the Electron Density, *Physical Review B*, **37(2):** 785–789 (1988).

[30] Miehlich B., Savin A., Stoll H., Preuss H., Results Obtained with the Correlation Energy Density Functionals of Becke and Lee, Yang and Parr, *Chemical Physics Letters*, **157(3):** 200–206 (1989).

[31] Reed A.E., Curtiss L.A., Weinhold F., Intermolecular Interactions from a Natural Bond Orbital, Donor-Acceptor Viewpoint, *Chemical Reviews*, **88(6):** 899–926 (1988).

[32] Wolinski K., Hinton J.F., Pulay P., Efficient Implementation of the Gauge-Independent Atomic Orbital Method for NMR Chemical Shift Calculations, *Journal of the American Chemical Society*, **112(23):** 8251–8260 (1990).

[33] Lodewyk M., Siebert M., Tantillo D., Computational Prediction of 1H and 13C Chemical Shifts: A Useful Tool for Natural Product, Mechanistic, and Synthetic Organic Chemistry, *Chemical Reviews*, **112(3):** 1839-1862 (2012).

[34] Morris G.M., Huey R., Lindstrom W., Sanner M.F., Belew R.K., Goodsell D.S., Olson A.J., AutoDock4 and AutoDockTools4: Automated Docking with Selective Receptor Flexibility, *Journal of Computational Chemistry*, **30(16):** 2785–2791 (2009).

[35] Daina A., Michielin O., Zoete V.,Swiss ADME: A Free Web Tool to Evaluate Pharmacokinetics, Drug-Likeness and Medicinal Chemistry Friendliness of Small Molecules, *Scientific Reports*, 7, 42717 (2017).

[36] Yang H., Lou C., Sun L., Li J., Cai Y., Wang Z., Li W., Liu G., Tang Y., AdmetSAR 2.0: Web-Service for Prediction and Optimization of Chemical ADMET Properties, *Bioinformatics*, **35(6):** 1067–1069 (2019).

[37] Lipinski C.A., Lombardo F., Dominy B.W., Feeney P.J., Experimental and Computational Approaches to Estimate Solubility and Permeability in Drug Discovery and Development Settings, *Advanced Drug Delivery Review*, **46(1–3):** 3–26 (2001).

[38] Veber D.F., Johnson S.R., Cheng H.-Y., Smith B.R., Ward K.W., Kopple K.D., Molecular Properties that Influence the Oral Bioavailability of Drug Candidates, *Journal of Medicinal Chemistry*, **45(12):** 2615–2623 (2002).

[39] Kesimli, B., Topacli, A., The Effects of Heating on the Molecular Structures of Cd and Co Complexes of Sulfamethoxazole, *Journal of Molecular Structure*, **561(1):** 55–59 (2001).

[40] Gorell J.M., Johnson C.C., Rybicki B.A., Peterson E.L., Kortsha G.X., Brown G.G., Richardson R.J., Occupational Exposure to Manganese, Copper, Lead, Iron, Mercury and Zinc and the Risk of Parkinson's Disease, *Neurotoxicology*, **20(2–3):** 239–247 (1999).

[41] Bouchoucha A., Zaater S., Bouacida S., Merazig H., Djabbar S., Synthesis and Characterization of New Complexes of Nickel (II), Palladium (II) and Platinum(II) with Derived Sulfonamide Ligand: Structure, DFT Study, Antibacterial and Cytotoxicity Activities, *Journal of Molecular Structure*, **1161:** 345–355 (2018).

[42] Aggarwal P., Tuli H.S., Kumar M., Novel Cyclic Schiff Base and Its Transition Metal Complexes: Synthesis, Spectral and Biological Investigations, *Iranian Journal of Chemistry and Chemical Engineering (IJCCE)*, **41(2):** 417–430 (2022).

[43] Bourouai M.A., Si Larbi K., Bouchoucha A., Terrachet-Bouaziz S., Djebbar S., New Ni(II) and Pd(II) Complexes Bearing Derived Sulfa Drug Ligands: Synthesis, Characterization, DFT Calculations, and in Silico and in Vitro Biological Activity Studies, *BioMetals*, **36:** 153-188 (2022).

[44] Krátký M., Dzurková M., Janoušek J., Konečná K., Trejtnar F., Stolaříková J., Vinšová J., Sulfadiazine salicylaldehyde-Based Schiff Bases: Synthesis, Antimicrobial Activity and Cytotoxicity, *Molecules*, **22(9):** 1573 (2017).

[45] Jr A., J, S., Rkr, A.-S., J, A., A, O., C, R., F, C., Ceftriaxone-based Schiff base Transition Metal(II) Complexes. Synthesis, Characterization, Bacterial Toxicity, and DFT Calculations. Enhanced Antibacterial Activity of a Novel Zn(II) Complex Against *S. aureus* and *E. coli*, *Journal of Inorganic Biochemistry*, **223:** 111519 (2021).

[46] D, D., N, S., S, R., P, D., S, M., El, T., C, S., The Crystal Structure of Sulfamethoxazole, Interaction with DNA, DFT Calculation, and Molecular Docking Studies, *Spectrochimica Acta. Part A, Molecular and Biomolecular Spectroscopy*, **137:** 560-568 (2015).

[47] Alyar S., Özmen Ü.Ö., Adem Ş., Alyar H., Bilen E., Kaya K., Synthesis, Spectroscopic Characterizations, Carbonic Anhydrase II Inhibitory Activity, Anticancer Activity and Docking Studies of New Schiff bases of Sulfa Drugs, *Journal of Molecular Structure*, **1223:** 128911 (2021).

[48] Sahu N., Mondal S., Sepay N., Gupta S., Torres-Lopez E., Tanaka S., Akitsu T., Sinha C., Antibacterial Activities of Sulfamethoxazolyl-azo-Phenols and their Cu(II) Complexes Along with Molecular Docking Properties, *Journal of Biological Inorganic Chemistry*, **22(6):** 833–850 (2017).

[49] Tercan M., Özdemir N., Özdemir F.A., Şerbetçi Z., Erdener D., Çetinkaya B., Dayan O., Synthesis, DFT Computations and Antimicrobial Activity of a Schiff base Derived from 2-Hydroxynaphthaldehyde: Remarkable Solvent Effect, *Journal of Molecular Structure*, **1209:** 127980 (2020).

[50] Mansour A.M., Coordination Behavior of Sulfamethazine Drug Towards Ru(III) and Pt(II) Ions: Synthesis, Spectral, DFT, Magnetic, Electrochemical and Biological Activity Studies, *Inorganica Chimica Acta*, **394:** 436–445 (2013).

[51] Zeyrek C.T., Ünver H., Arpacı Ö.T., Polat K., İskeleli N.O., Yildiz M., Experimental and Theoretical Characterization of the 2-(4-Bromobenzyl)-5-Ethylsulphonyl-1,3-Benzoxazole, *Journal of Molecular Structure*, **1081:** 22–37 (2015).

[52] Zaater S., Bouchoucha A., Djebbar S., Brahimi M., Structure, Vibrational Analysis, Electronic Properties and Chemical Reactivity of Two Benzoxazole Derivatives: Functional Density Theory Study, *Journal of Molecular Structure*, **1123:** 344–354 (2016).

[53] Hora Machado A.E.D., Miranda J.A.D., Guilardi S., Nicodem D.E., Severino D., Photophysics and Spectroscopic Properties of 3-Benzoxazol-2-yl-Chromen-2-One, *Spectrochimica Acta Part A: Molecular and Biomolecular Spectroscopy*, **59(2):** 345–355 (2003).

[54] Chen S.-L., Liu Z., Liu J., Han G.-C., Li Y.-H., Synthesis, Characterization, Crystal Structure and Theoretical Approach of Cu(II) Complex with 4-{(Z)-(2-Hydroxybenzoyl)Hydrazono]Methyl}Benzoic Acid, *Journal of Molecular Structure*, **1014:** 110–118 (2012).

[55] Bensouilah N., Fisli H., Dhaoui N., Benali-Cherif N., Abdaoui M., Solvent Effects of N-Nitroso, N-(2-Chloroethyl), N',N'-Dibenzylsulfamid and its Copper(II) and Cobalt(II) Complexes: Fluorescence Studies, *Luminescence: The Journal of Biological and Chemical Luminescence*, **28(1):** 30–37 (2013).

[56] Balaban Gündüzalp A., Özbek N., Karacan N., Synthesis, Characterization, and Antibacterial Activity of the Ligands Including Thiophene/Furan Ring Systems and their Cu(II), Zn(II) Complexes, *Medicinal Chemistry Research*, **21(11):** 3435–3444 (2012).

[57] Pang Z., Raudonis R., Glick B.R., Lin T.-J., Cheng Z., Antibiotic Resistance in Pseudomonas Aeruginosa: Mechanisms and Alternative Therapeutic Strategies, *Biotechnology Advances*, **37(1):** 177–192 (2019).

[58] Hassan S.A., Aziz D.M., others, Synthesis, in Vitro Antimicrobial Assay and Molecular Docking Studies of some New Symmetrical Bis-Schiff Bases and their 2-Azetidinones., *Zanco Journal of Pure and Applied Sciences*, **33(2):** 34-50 (2021).

[59] Smilack J.D., Trimethoprim-Sulfamethoxazole, *Mayo Clinic Proceedings*, **74(7):** 730–734 (1999).

[60] Chaffin W.L., Candida Albicans Cell Wall Proteins, *Microbiology and Molecular Biology Reviews: MMBR*, **72(3):** 495–544 (2008).

[61] Achari A., Somers D.O., Champness J.N., Bryant P.K., Rosemond J., Stammers D.K., Crystal Structure of the Anti-Bacterial Sulfonamide Drug Target Dihydropteroate Synthase, *Nature Structural Biology*, **4(6):** 490–497 (1997).

[62] Hampele I.C., D'Arcy A., Dale G.E., Kostrewa D., Nielsen J., Oefner C., Page M.G., Schönfeld H.-J., Stüber D., Then R.L., Structure and Function of the Dihydropteroate Synthase from Staphylococcus Aureus. *Journal of Molecular Biology*, **268(1):** 21–30 (1997).

[63] Pal S., Kumar V., Kundu B., Bhattacharya D., Preethy N., Reddy M.P., Talukdar A., Ligand-Based Pharmacophore Modeling, Virtual Screening and Molecular Docking Studies for Discovery of Potential Topoisomerase I Inhibitors, *Computational and Structural Biotechnology Journal*, **17:** 291–310 (2019).

[64] Hajji H., others, Antiproliferative Activity: Discovery of new Benzoxanthenes derivatives by Using Various Statistical Methods 2D/3D-QSAR and Molecular Docking, *RHAZES: Green and Applied Chemistry*, **12:** 40–59 (2021).

[65] Aqeel A.M., Jamil M.M., Yusuf I., Synthesis, Characterization and Biological Studies of 2-(4-Nitrophenylaminocarbonyl)Benzoic Acidand Its Complexes with Cr(III), Co(II), Ni(II), Cu(II) and Zn(II), *Iranian Journal of Chemistry and Chemical Engineering (IJCCE)*, **31(1):** 9-14 (2012).

[66] Eze F.U., Okoro U.C., Ukoha P.O., Ugwu D.I., New Antioxidant Agents Bearing Carboxamide Moiety: Synthesis, Molecular Docking and in Vitro Studies of New Benzenesulfonamide Derivatives, *Iranian Journal of Chemistry and Chemical Engineering (IJCCE)*, **40(3):** 853-865 (2021).